

Superconductivity with high upper critical field in Ta-Hf Alloys

P. K. Meena,¹ S. Jangid,¹ R. K. Kushwaha,¹ and R. P. Singh^{1,*}

¹*Department of Physics, Indian Institute of Science Education and Research Bhopal, Bhopal, 462066, India*

High upper-critical field superconducting alloys are required for superconducting device applications. In this study, we extensively characterized the structure and superconducting properties of alloys $\text{Ta}_x\text{Hf}_{1-x}$ ($x = 0.2, 0.4, 0.5, 0.6$ and 0.8). The substitution of Hf ($T_C = 0.12$ K, type-I superconductor) with Ta ($T_C = 4.4$ K, type-I superconductor) shows an anomalous enhancement of T_C with variation of composition. Interestingly, all compositions exhibited strongly coupled bulk type-II superconductivity with a high upper critical field. In particular, for compositions $x = 0.2$, and 0.4 , the upper critical field (H_{C2}) approached the Pauli limiting field.

I. INTRODUCTION

Superconductivity, a quantum phenomenon with significant practical applications, has recently led to the exploration of unconventional superconductors that exhibit remarkable properties that differ from the conventional Bardeen-Cooper-Schrieffer (BCS) model [1]. These unconventional superconductors exhibit remarkable features, such as an upper critical field comparable to or exceeding the Pauli paramagnetic field, strong electron-phonon interactions, the presence of gap nodes, and the breaking of time-reversal symmetry (TRS) [2, 3]. The strength of spin-orbit coupling (SOC) in the materials under investigation plays a pivotal role in the emergence of unconventional superconductivity [4–10]. Superconductors based on heavier elements with higher atomic numbers, particularly those in the 5d series, tend to exhibit robust spin-orbit coupling ($\text{SOC} \propto Z^4$), giving rise to these unconventional superconducting behaviors [11–17].

The Ta-Hf binary alloy is a notable example of a 5d superconducting alloy that combines two type-I superconductors, Ta and Hf. It is anticipated to exhibit strong spin-orbit coupling due to the high atomic numbers of its constituent elements. Surprisingly, this alloy displays remarkable behavior in the upper critical field. By partially substituting Hf for Ta, it is possible to modify the strength of spin-orbit coupling [18]. When Hf atoms are introduced into Ta, which has a T_C of 4.2 K, the superconducting transition temperature increases to 6.7 K in the Hf-Ta alloy with approximately 40 % Hf [19]. The relationship between the density of states at the Fermi level, the electron-phonon coupling, and the number of valence electrons (d shell) per atom has been correlated with the superconducting transition temperature (T_C) [20, 21]. However, T_C exhibits non-monotonic behavior with valence electron counts, a trend observed in other binary alloy superconductors [20, 22–28]. These metallic alloys possess both metallic properties and a high upper critical field, making them highly promising for practical

superconducting devices.

Despite studies on Ta-Hf binary alloys [29, 30], the mechanisms responsible for the enhanced critical temperature (T_C) and the high upper critical field behavior in these alloys have not been fully understood, primarily due to incomplete characterization. Unravelling these mechanisms could provide valuable insight and enable the synthesis of metallic alloys with enhanced properties suitable for practical applications. Thus, the Ta-Hf alloy is a promising candidate for in-depth investigations into its superconducting properties, offering a platform to better comprehend other binary superconducting behaviours.

In this study, we investigate the superconducting properties of binary $\text{Ta}_x\text{Hf}_{1-x}$ alloys, where x takes values of 0.2, 0.4, 0.5, 0.6, and 0.8. Our analysis included electrical resistivity, DC magnetization, and heat capacity measurements, allowing us to construct the phase diagram for these alloys. Throughout the entire range of the solid solution, we observed the coexistence of two crystal structures: W-*bcc* and Mg-*hcp*. Importantly, all compositions of $\text{Ta}_x\text{Hf}_{1-x}$ exhibited bulk type-II superconductivity. Notably, the presence of strongly coupled superconductivity and an upper critical field comparable to the Pauli limiting field suggests the potential occurrence of unconventional superconductivity.

II. EXPERIMENTAL DETAILS

Polycrystalline samples of $\text{Ta}_x\text{Hf}_{1-x}$ were prepared by arc melting using high-purity Ta(99.99%) and Hf(99.99%) metals in stoichiometric ratios in a high-purity Ar(99.99%) environment on a water-cooled copper hearth. Ingots were repeatedly remelted and flipped to enhance chemical homogeneity with minimal mass loss. A titanium button was used as a getter to remove residual oxygen in the chamber. Crystal structure and phase purity were verified using powder X-ray diffraction (PXRD) on a PANalytical diffractometer equipped with CuK_α radiation ($\lambda = 1.54056$ Å). Magnetization measurements were performed using the Magnetic Property Measurement System (MPMS3; Quantum Design). Specific heat and electrical resistivity measurements were carried out using the Physical Property Measurement System (PPMS; Quantum Design).

* rpsingh@iiserb.ac.in

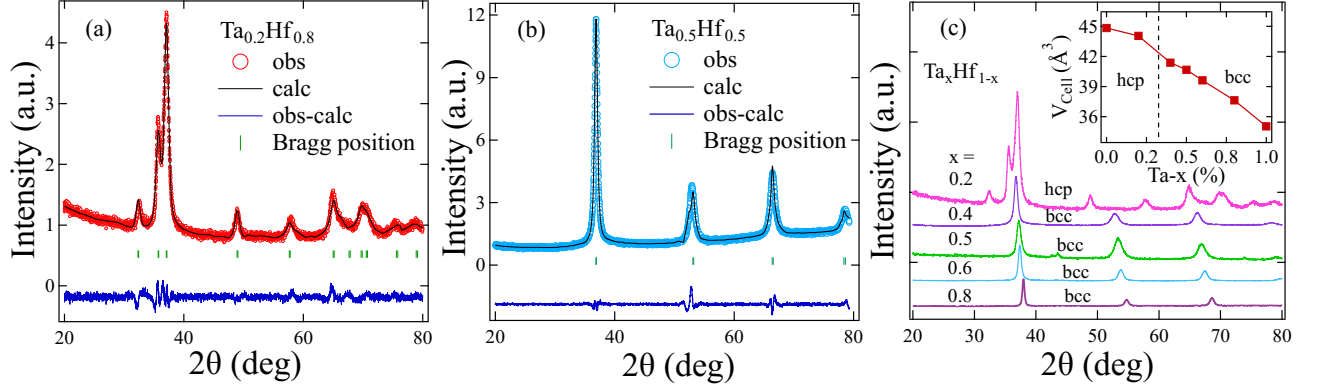


FIG. 1. Powder XRD patterns with refinement for binary alloys, (a) $\text{Ta}_{0.2}\text{Hf}_{0.8}$. (b) $\text{Ta}_{0.5}\text{Hf}_{0.5}$. (c) All compositions XRD patterns for $\text{Ta}_x\text{Hf}_{1-x}$. The inset shows the refined cell volume as a function of the Ta content x .

III. EXPERIMENTAL RESULTS

a. Sample characterization

All synthesized $\text{Ta}_x\text{Hf}_{1-x}$ alloys (with $x = 0.2, 0.4, 0.5, 0.6$, and 0.8) are found to be in a pure phase and crystallize into two distinct crystal structures. Fig. 1(a,b) shows representative XRD patterns for polycrystalline binary alloys with $x = 0.2$ and 0.5 , while the XRD patterns of other alloys closely resemble those of $x = 0.5$. We used FullProf Rietveld software [31] to analyze the XRD patterns, revealing that the samples can be well indexed by the Mg-*hcp* structure with space group $P6_3/mmc$ for $x = 0.2$ and the W-*bcc* structure with space group $Im\bar{3}m$ for the remaining compositions. Fig. 1(c) displays the XRD patterns for all compounds ($x = 0.2, 0.4, 0.5, 0.6$, and 0.8), while the refined structural lattice parameters for these compounds are summarized in Table I. The lattice constants obtained for some binary compounds are consistent with previous studies in the literature [32], whereas others are reported for the first time in this work. The inset of Fig. 1(c) shows a linear decrease in V_{cell} with increasing x , which can be attributed to the smaller atomic radius of Ta compared to Hf.

b. Superconducting and normal state properties

Superconductivity in the $\text{Ta}_x\text{Hf}_{1-x}$ alloys (where $x = 0.2, 0.4, 0.5, 0.6$, and 0.8) was confirmed by measurements of electrical resistivity and DC magnetization. Temperature-dependent electrical resistivity ($\rho(T)$) was measured from 300 K to 1.9 K at zero magnetic field ($H = 0$ mT), as shown in Fig. 2(a). The resistivity exhibited a slight temperature variation above the superconducting transition temperature (T_C), indicating the weak metallic character of the Ta-Hf alloys [33, 34]. The values of the residual resistivity ratio (RRR), defined as the ratio of resistivity at 300 K to that at 8 K, were found to be relatively small ($\text{RRR} \simeq 1\text{-}2$) for all compositions, sug-

gesting the presence of disorder in the binary alloy. The RRR values follow a similar pattern observed in other binary alloys [35] and are provided in Table I. Fig. 2(b) presents an expanded plot of the normalized electrical resistivity data at zero field, clearly showing the superconducting transitions corresponding to different compositions of the Ta-Hf alloy. The superconducting transition temperature (T_C) varies non-linearly with the Hf (or Ta) concentration, ranging from 0.12 K for pure Hf to 6.7 K for a Ta concentration of 60% in solid solution, with a T_C of 4.2 K for pure Ta.

The magnetic moment variations with temperature were measured at an applied field of 1.0 mT using two different modes: zero-field cooled warming (ZFCW) and field-cooled cooling (FCC). Magnetization data for all samples exhibited the emergence of diamagnetic behavior at different transition temperatures (T_C), consistent with resistivity measurements, as shown in Fig. 2(c). The Ta-Hf binary alloy displayed a distinct dome-shaped behavior, similar to that observed in the Ti-V [36] and Zr-Nb [37] binary alloys. The maximum and minimum T_C values of 6.7 K and 4.5 K were observed for compositions corresponding to 60% and 20% Ta concentration, respectively. The separation between the ZFCW and FCC modes in the magnetization data below T_C indicates a strong magnetic flux pinning. The respective T_C values obtained from DC magnetization consistent with the electrical transport measurements and values are summarized in Table I.

Magnetization versus field (M-H) measurements were conducted for $\text{Ta}_x\text{Hf}_{1-x}$ alloys to confirm their type-II behavior. Fig. 3(a) displays the M-H curves for $x = 0.4, 0.5$, and 0.6 , revealing the presence of the fishtail effect. The composition $x = 0.5$ also exhibits a flux jump in the magnetization loop. These unconventional vortex states, typically observed in high- T_C oxides and certain two-dimensional superconducting materials [38–41], suggest the influence of strong disorder in the material.

The lower critical field, $H_{C1}(0)$, was estimated by measuring the low field M-H. The temperature dependence of

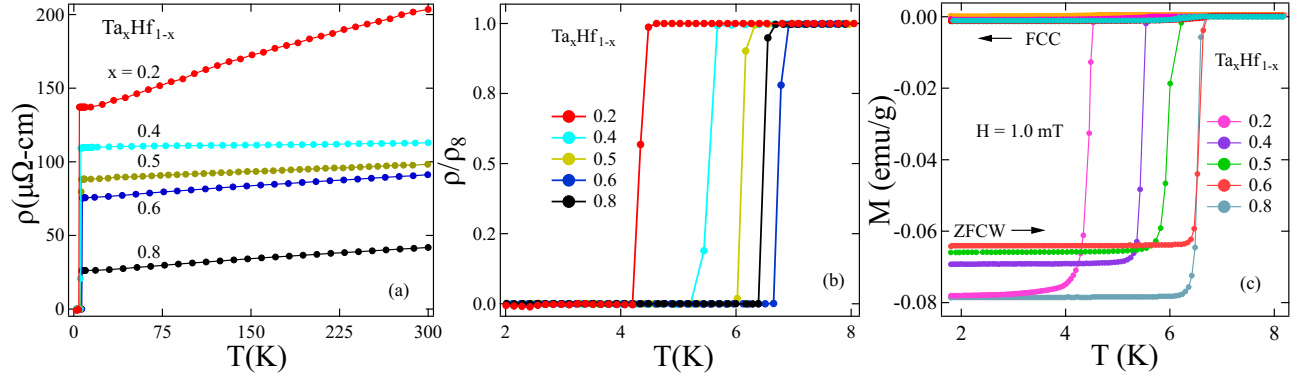


FIG. 2. (a) Temperature variation of electrical resistivity $\rho(T)$ at $H = 0 \text{ mT}$ for $\text{Ta}_x\text{Hf}_{1-x}$ ($x = 0.2, 0.4, 0.5, 0.6$, and 0.8). (b) A zoomed-in view of the normalized resistivity (ρ/ρ_8) highlights the superconducting drop observed in all compositions. (c) Magnetization data obtained during field-cooled cooling (FCC) and zero field-cooled heating (ZFCW) measurements in an applied field of $H = 1.0 \text{ mT}$ show the presence of superconductivity below T_C for all binary $\text{Ta}_x\text{Hf}_{1-x}$ compositions.

H_{C1} is determined by identifying the point at which the $M(H)$ curves deviate from the Meissner line, as shown in the inset of Fig. 3(b) for $\text{Ta}_{0.5}\text{Hf}_{0.5}$. The temperature variation of the H_{C1} values for all compositions is presented in Fig. 3(b). Utilizing the Ginzburg-Landau (GL) theory of phase transition, $H_{C1}(0)$ values for $\text{Ta}_x\text{Hf}_{1-x}$ can be obtained by fitting the expression for $H_{C1}(T)$,

$$H_{C1}(T) = H_{C1}(0) \left[1 - \left(\frac{T}{T_C} \right)^2 \right]. \quad (1)$$

The estimated $H_{C1}(0)$ is in the range of 20-30 mT for all compositions of $\text{Ta}_x\text{Hf}_{1-x}$ ($x = 0.2, 0.4, 0.5, 0.6$, and 0.8). Temperature-dependent magnetization and resistivity data were also taken in various applied external magnetic fields up to 7.0 T and 9.0 T, respectively, to determine the upper critical field $H_{C2}(0)$. The observed changes in T_C with the increasing applied magnetic field, as shown in the inset of Fig. 3(c) for $\text{Ta}_{0.5}\text{Hf}_{0.5}$, are interpreted as the upper critical field $H_{C2}(T)$. Temperature-dependent H_{C2} data were fitted using Ginzburg-Landau (GL) expression for respective compositions to determine the $H_{C2}(0)$ values as given in Eq. (2) and the fitting is shown by solid lines in Fig. 3(c).

$$H_{C2}(T) = H_{C2}(0) \left[\frac{(1 - t^2)}{(1 + t^2)} \right], \quad \text{where } t = \frac{T}{T_C} \quad (2)$$

The estimated $H_{C2}(0)$ values through aforementioned measurements are given in the Table I for all the composite alloys. Maximum $H_{C2}(0)$ values are obtained as 10.43 T for $\text{Ta}_{0.4}\text{Hf}_{0.6}$ and exhibit a steady decrease with increasing Ta content in replacement of Hf content [29].

In type-II superconductors, the presence of a magnetic field leads to the destruction of superconductivity due to two main effects: the orbital limiting field and the Pauli paramagnetic field. In situations where both effects are significant, the temperature dependence of the

upper critical field can be described by the Werthamer-Helfand-Hohenberg (WHH) theory. This theory considers the combined influences of spin paramagnetism and spin-orbit interaction. In the absence of Pauli spin paramagnetism and the spin-orbit interaction, the WHH theory provides the following equation [42, 43]:

$$H_{C2}^{orb}(0) = -\alpha T_C \left. \frac{dH_{C2}(T)}{dT} \right|_{T=T_C} \quad (3)$$

which gives the orbital limit field of the Cooper pair. The constant α , is the purity factor of 0.693(0.73) for dirty(clean) limit superconductors. For the dirty limit condition, we obtained the $H_{C2}^{orb}(0)$ values, which are summarized in Table I. But the latter λ_{SO} has been shown to increase with increasing atomic numbers of the composing elements [30] and is thus expected to be high for $\text{Ta}_x\text{Hf}_{1-x}$, so the spin-orbit scattering effect cannot be ignored. However, the Pauli limit of the upper critical field [44, 45], can be calculated by following relation $H_{C2}^p(0) = 1.84 T_C$ within the BCS theory. We calculated the $H_{C2}^p(0)$ values using the estimated T_C of the resistivity curves as 8.28, 10.34, 11.59, 12.32, 12.14 T for $\text{Ta}_x\text{Hf}_{1-x}$ ($x = 0.2, 0.4, 0.5, 0.6$, and 0.8). Interestingly, the value of $H_{C2}(0)$ is comparable to Pauli's limiting field for $x = 0.2, 0.4$, indicating the unconventionality present in these compounds. Similar results have been observed in certain superconductors, including Chevrel phase [46], A15 compounds [47], and various Re-based noncentrosymmetric superconductors [48–50]. To further quantify the impact of spin paramagnetic effects, we calculated the Maki parameter (α_m), which is given in the following expression:

$$\alpha = \sqrt{2} \frac{H_{C2}^{orb}(0)}{H_{C2}^p(0)} \quad (4)$$

The calculated values of α_m are provided in Table I. The observed variation of α_m with doping can be attributed to the interplay between spin-orbit coupling and doping-induced disorder, arising from differences in

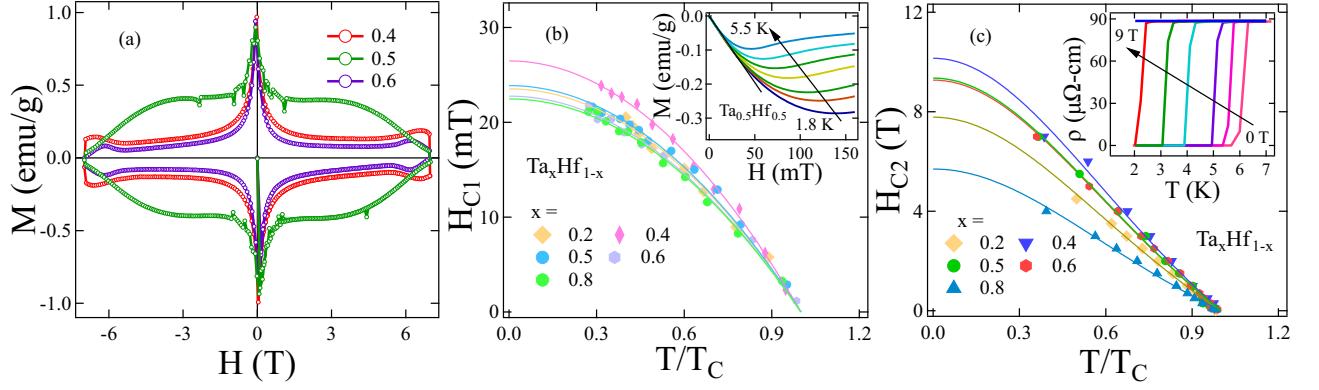


FIG. 3. (a) The magnetization of $\text{Ta}_x\text{Hf}_{1-x}$ alloys was measured in the magnetic field range of -7 T to 7 T. The fishtail effect near a magnetic field of 6 T is evident in the data. (b) The temperature dependence of the lower critical field (H_{C1}) was determined from magnetization measurements. The H_{C1} values were fitted using the Ginzburg-Landau (GL) equation for $\text{Ta}_x\text{Hf}_{1-x}$ alloys. The inset shows the magnetization curve ($M(H)$) for $\text{Ta}_{0.5}\text{Hf}_{0.5}$ at various temperatures. (c) The temperature dependence of the upper critical field (H_{C2}) was obtained from resistivity measurements. The H_{C2} values were fitted using the GL equation. The inset shows the temperature-dependent resistivity ($\rho(T)$) for $\text{Ta}_{0.5}\text{Hf}_{0.5}$ at different magnetic fields.

atomic numbers (Z) and atomic radii of the constituent elements in the Ta-Hf alloy. Two length scales of characteristics of a superconductor were determined: penetration depth $\lambda_{GL}(0)$ and Ginzburg-Landau coherence length $\xi_{GL}(0)$ from the given relations using the value of $H_{C1}(0)$ and $H_{C2}(0)$,

$$H_{C2}(0) = \frac{\Phi_0}{2\pi\xi_{GL}^2(0)}, \quad (5)$$

$$H_{C1}(0) = \frac{\Phi_0}{4\pi\lambda_{GL}^2(0)} \left(\ln \frac{\lambda_{GL}(0)}{\xi_{GL}(0)} + 0.12 \right); \quad (6)$$

where Φ_0 denotes the fluxoid quantum ($\Phi_0 = 2.07 \times 10^{-15} \text{ T m}^2$) [51]. Subsequently, the GL parameter is defined as $k_{GL} = \frac{\lambda_{GL}(0)}{\xi_{GL}(0)}$, which signifies the type of superconductivity (either I or II), was also calculated for each composition. Moreover, the relation $H_{C1}(0)H_{C2}(0) = H_C^2(0) \ln(k_{GL}(0) + 0.08)$ can be used to compute thermodynamic critical field H_C at 0 K using the value of $H_{C1}(0)$, $H_{C2}(0)$ and k_{GL} . The obtained values of H_C are 190-300 mT for all compositions. All physical parameters $\xi_{GL}(0)$, $\lambda_{GL}(0)$, and k_{GL} are summarized in Table I. The estimated values of $\xi_{GL}(0)$ and $\lambda_{GL}(0)$ are in the range of 5-8 nm and 140-160 nm, respectively, same as Re-doped MoTe_2 [52], Ru and Ir doped LaRu_3Si_2 [53]. The large values of k_{GL} in the range of 23-27 [54] for binary compounds, suggests that $\text{Ta}_x\text{Hf}_{1-x}$ have strong type-II superconductivity.

Heat capacity measurements were conducted for all compositions to further characterize superconductivity in $\text{Ta}_x\text{Hf}_{1-x}$ alloys. As depicted in Figure 4, the heat capacity plots exhibit a discontinuity that signifies the transition from normal to superconducting state. The determined T_C values of the specific heat are consistent with

all the resistivity and magnetization measurements of the compounds. Low-temperature specific heat can be described using the Debye relation, $C = \gamma_n T + \beta T^3$, where the term $\gamma_n T$ represents the electronic contribution, and the term βT^3 corresponds to the phononic contribution. By extrapolating the behavior of the normal state to low temperatures, the Sommerfeld coefficient (γ_n) and the Debye constant (β) can be estimated.

Using the known value of β , the Debye temperature θ_D can be calculated using the expression $\theta_D = \left(\frac{12\pi^4 R n}{5\beta} \right)^{\frac{1}{3}}$, where R is the universal gas constant ($8.314 \text{ J K}^{-1} \text{ mol}^{-1}$) and $n = 1$ is the number of atoms per unit cell. The density of states (DOS) at the Fermi level, denoted as $D(E_F)$, can be determined using the rela-

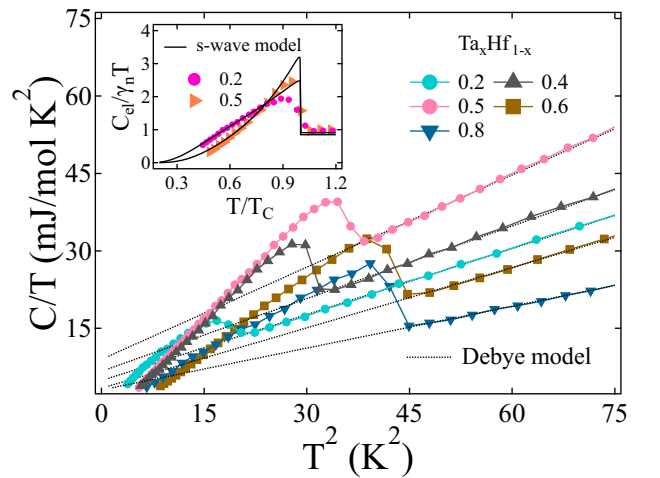


FIG. 4. C/T versus T^2 measured at $H = 0 \text{ mT}$ and fitted in normal state using relation $C = \gamma_n T + \beta T^3$. Inset shows normalized electronic specific heat, which is well described with the isotropic BCS model.

TABLE I. $\text{Ta}_x\text{Hf}_{1-x}$ ($x = 0.2 - 0.8$) Space group, refined lattice parameters, and cell volume derived from X-ray refinement as well as superconducting and normal-state parameters derived from magnetization, resistivity, and specific heat measurements.

Parameter	unit	0.2	0.4	0.5	0.6	0.8
Space group		$P6_3/mmc$		$Im\bar{3}m$		
a = b	Å	3.1849	3.4586	3.4392	3.4034	3.3509
c	Å	5.0143	3.4586	3.4392	3.4034	3.3509
V_{cell}	Å ³	44.05	41.37	40.67	39.62	37.62
T_C	K	4.5	5.6	6.1	6.7	6.6
$H_{C1}(0)$	mT	23.52	26.40	23.87	22.6	22.51
$H_{C2}^{res}(0)$	T	7.72	10.43	9.3	9.27	5.69
$H_{C2}^P(0)$	T	8.28	10.34	11.59	12.32	12.14
$H_{C2}^{orb}(0)$	T	3.34	5.89	6.77	6.30	3.68
α_m		0.56	0.80	0.82	0.72	0.43
ξ_{GL}	nm	6.52	5.62	5.95	5.96	7.60
λ_{GL}^{mag}	nm	150.74	144.64	151.93	156.84	149.19
k_{GL}		23.07	25.73	25.53	26.31	19.63
$\rho_{300K}/\rho_{8K}(\text{RRR})$		1.48	1.02	1.11	1.20	1.59
γ_n	mJ mol ⁻¹ K ⁻²	4.44	5.87	7.76	3.51	3.32
θ_D	K	164.66	158.73	146.50	170.92	190.20
$\frac{\Delta_{sp}(0)}{k_B T_C}$		1.87	2.56	2.45	2.61	2.14
λ_{e-ph}		0.75	0.84	0.91	0.88	0.82
$\frac{m^*}{m_e}$		0.7	0.8	0.94	0.6	0.58
v_f	10 ⁵ ms ⁻¹	7.54	7.61	7.19	8.11	8.15
$\frac{\xi_0}{l_e}$		2.7	3.58	4.87	2.66	2.15
$\frac{T_C}{T_F}$		0.00034	0.00036	0.00038	0.00051	0.00051

tion $D(E_F) = \frac{3\gamma_n}{\pi^2 k_B^2}$, where k_B is the Boltzmann constant [55]. By applying these equations, the calculated values of θ_D are lower than the Debye temperature of the corresponding elements. Furthermore, as the concentration increases up to 50% of the Ta content, the values of θ_D decrease, indicating that doping introduces some disorder in binary alloys. The values obtained from θ_D are provided in Table I. Subsequently, we determined the electron-phonon coupling constant, denoted as λ_{e-ph} . This dimensionless constant quantifies the attractive interaction between electrons and phonons and can be calculated using the values of T_C and θ_D through the semi-empirical McMillan formula [56],

$$\lambda_{e-ph} = \frac{1.04 + \mu^* \ln(\theta_D/1.45T_C)}{(1 - 0.62\mu^*) \ln(\theta_D/1.45T_C) - 1.04}. \quad (7)$$

where the repulsive screened Coulomb parameter, denoted as μ^* , typically falls within the range of 0.09 to 0.18, with a commonly used value of 0.13 for intermetallic compounds. In our case, we adopted a value of 0.13. The estimated values of λ_{e-ph} for $\text{Ta}_x\text{Hf}_{1-x}$ alloys range from 0.7 to 1, as summarized in Table I. Similar values of λ_{e-ph} have been observed in other binary compounds, such as $\text{Re}_{1-x}\text{Mo}_x$ [57]. The higher values of λ_{e-ph} in $\text{Ta}_x\text{Hf}_{1-x}$ alloys indicate a strong coupling strength among electrons in the superconducting state [58].

The inset of Fig. 4 presents the electronic component of the specific heat, denoted as C_{el} (shown for $x = 0.2$ and

0.5), which was obtained by subtracting the contribution of the phonon from the experimental data using the relation $C_{el}(T) = C - \beta T^3$. The $C_{el}(T)$ data for all compositions are well described by the isotropic s-wave model in the BCS theory, as outlined in ref. [59]. The black line in the inset of Fig. 4 represents the curve fitted to the data using the single-gap s-wave BCS equation. The values obtained from the superconducting gap ($\frac{\Delta(0)}{k_B T_C}$), listed in Table I, exceed the predicted BCS value, indicating the presence of strongly coupled superconductivity in $\text{Ta}_x\text{Hf}_{1-x}$ compounds.

c. Electronic properties and the Uemura classification

The Sommerfeld coefficient γ_n , is related to the effective mass of quasi-particles m^* and electronic carrier density n of the system by the following expression [55],

$$\gamma_n = \left(\frac{\pi}{3}\right)^{2/3} \frac{k_B^2 m^* V_{f.u.} n^{1/3}}{\hbar^2 N_A} \quad (8)$$

where $k_B = 1.38 \times 10^{-23}$ J/K is the Boltzmann's constant, N_A and $V_{f.u.}$ are the Avogadro number and the volume of a formula unit, respectively. The following relations can be used to connect the electronic mean free path l_e and the carrier density n to the Fermi velocity v_F and the effective mass m^* ,

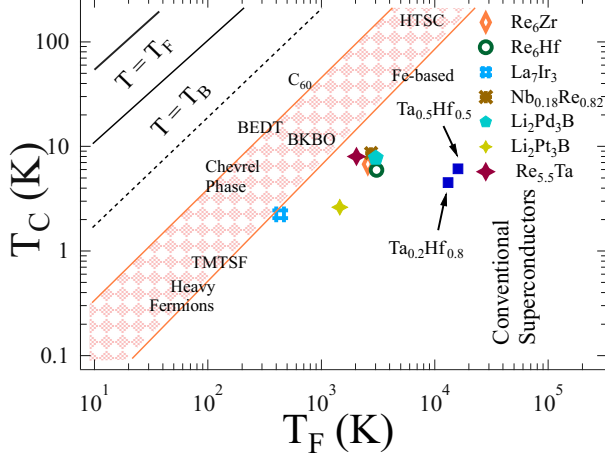


FIG. 5. An "Uemura plot" showing superconducting transition temperature (T_C) versus effective Fermi temperature (T_F), in which blue square symbols representing the positions of $\text{Ta}_x\text{Hf}_{1-x}$. The data point is inside two solid boundary lines depicting the unconventional zone.

$$l_e = \frac{3\pi^2\hbar^3}{e^2\rho_0 m^{*2}v_F^2}, \quad n = \frac{1}{3\pi^2} \left(\frac{m^*v_F}{\hbar} \right)^3 \quad (9)$$

In the dirty limit, the GL penetration depth $\lambda_{GL}(0)$ and coherence length $\xi_{GL}(0)$ get affected, which can be described in terms of London penetration depth (λ_L) and BCS coherence length (ξ_0), by the following modified Eqs.10 and Eqs.11, respectively,

$$\lambda_{GL}(0) = \lambda_L \left(1 + \frac{\xi_0}{l_e} \right)^{1/2}, \quad \lambda_L = \left(\frac{m^*}{\mu_0 n e^2} \right)^{1/2} \quad (10)$$

$$\frac{\xi_{GL}(0)}{\xi_0} = \frac{\pi}{2\sqrt{3}} \left(1 + \frac{\xi_0}{l_e} \right)^{-1/2} \quad (11)$$

The above set of Eqs.(8-11) were solved simultaneously as done in Ref. [60] to evaluate the electronic parameters n , m^* , ξ_0 and l_e using the values of γ_n , $\xi_{GL}(0)$, and ρ_0 for varying the chemical compositions of $\text{Ta}_x\text{Hf}_{1-x}$. Finally, the effective Fermi temperature (T_F) for $\text{Ta}_x\text{Hf}_{1-x}$ was calculated using the expression [61], where n and m^* are the electronic carrier density and the effective mass of quasi-particles, respectively:

$$k_B T_F = \frac{\hbar^2}{2} (3\pi^2)^{2/3} \frac{n^{2/3}}{m^*}, \quad (12)$$

We have compiled all the estimated electronic parameters of $\text{Ta}_x\text{Hf}_{1-x}$ in Table I. The ratio ξ_0/l_e exceeds the expected range for clean limit superconductivity, indicating that the Ta-Hf binary alloy exhibits dirty limit superconductivity.

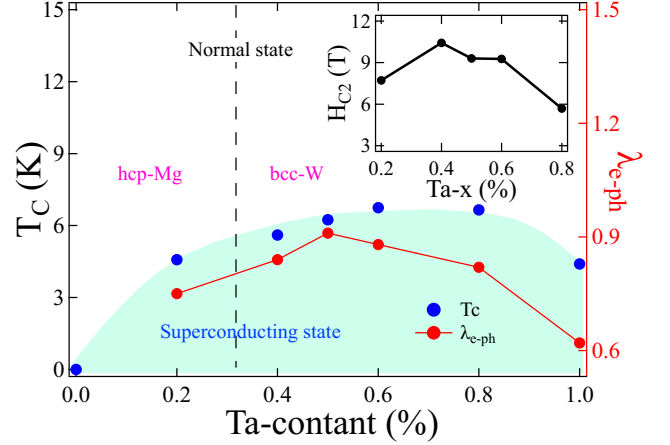


FIG. 6. Superconducting phase diagram of the $\text{Ta}_x\text{Hf}_{1-x}$ alloys. Superconducting transition temperatures T_C and electron-phonon coupling λ_{e-ph} vs Ta content. Inset shows a variation of an upper critical field with changing Ta content.

Uemura et al. [62] have established a distinction between conventional and unconventional superconductors based on the $\frac{T_C}{T_F}$ ratio. When this ratio falls within the range of $0.01 \leq \frac{T_C}{T_F} \leq 0.1$, the material is classified as an unconventional superconductor. Unconventional superconductors encompass various superconducting compounds, including heavy fermionic materials, Chevrel phases, high T_C superconductors, iron-based superconductors, and other exotic superconductors. The boundary for unconventional superconductors is represented by two solid peach lines in Fig. 5, and the values of $\frac{T_C}{T_F}$ for each composition (indicated by the blue symbols) lie between 0.00034 and 0.00052. These values position the $\text{Ta}_x\text{Hf}_{1-x}$ compounds outside the unconventional superconductivity region.

IV. PHASE DIAGRAM

The experimental data obtained from the superconducting $\text{Ta}_x\text{Hf}_{1-x}$ binary alloys are summarized in the phase diagram shown in Fig. 6. As the relative content of Ta and Hf is varied, two crystal structures are observed: W-bcc ($Im\bar{3}m$) and Mg-hcp ($P6_3/mmc$). Crystal structure transitions occur between $x = 0.2$ and 0.4 at the phase boundary. The highest and lowest values of T_C , 6.7 K and 4.5 K, respectively, are obtained for samples with $x = 0.6$ (W cubic-type structure) and $x = 0.2$ (Mg-hcp type structure), as depicted in Fig. 6. The variation of x on both sides leads to a decrease in the transition temperature, which can be attributed to the influence of elemental Ta and Hf on their respective sides [63, 64].

The phase diagram also shows the variation of the electron-phonon coupling constant with the Ta content, exhibiting a dome-like behavior. The three series of BCC alloys (3d, 4d, 5d) demonstrate the same dome behavior,

with a peak at a valence electron/atom ratio $n = 4.5$, a deep minimum near $n = 5.8$, and a shoulder at $n = 6.2$ [56]. The enhanced values of the electron-phonon coupling constant in Ta-Hf binary alloys are also higher than those of the elemental Hf and Ta, indicating strongly coupled superconductivity. The inset of Fig. 6 illustrates the variation between the upper critical field $H_{C2}(0)$ and the Ta/Hf concentration. A similar trend has been observed in previous studies of other binary solid solution alloys [65]. $\text{Ta}_{0.4}\text{Hf}_{0.6}$ corresponds to the highest value of $H_{C2}(0)$, which is 10.43 T (comparable to the Pauli paramagnetic limit), and as the concentration of Ta increases, $H_{C2}(0)$ decreases in the phase diagram.

V. CONCLUSION

This study presents experimental results focusing on $\text{Ta}_x\text{Hf}_{1-x}$ ($x = 0.2, 0.4, 0.5, 0.6, 0.8$) binary alloys. Through powder X-ray diffraction (XRD) analysis, it was determined that the crystal structures of $\text{Ta}_x\text{Hf}_{1-x}$ alloys encompass two phases across the entire range of solid solution: *W-bcc* (for $x \geq 0.4$) and *Mg-hcp* (for $x < 0.4$). Investigation of magnetization, electrical transport, and thermodynamic properties revealed that $\text{Ta}_x\text{Hf}_{1-x}$ alloys exhibit superconductivity, with the highest bulk transition temperature observed at $T_C = 6.7$ K for the composition $x = 0.6$. Significantly higher calculated values of the upper critical field $H_{C2}(0)$ were obtained, particularly for $x = 0.2$ and 0.4 , indicating their proximity to the BCS Pauli limiting field. Furthermore, analysis of the low-temperature specific heat data indicated a fully gapped superconducting state, with a larger gap magnitude exceeding the BCS value of 1.76. This magnitude is comparable to unconventional superconductors based on 5d compounds, suggesting an enhanced electron-phonon coupling constant in $\text{Ta}_x\text{Hf}_{1-x}$ alloys. The unique characteristics of $\text{Ta}_x\text{Hf}_{1-x}$ alloys, such as their higher upper critical fields, the presence of a fishtail characteristic (indicating unusual lattice vortices), larger superconducting gap values and strong electron-phonon coupling, suggest possible unconventional behaviour and make them intriguing for potential applications in superconducting devices. However, further investigations are necessary using microscopic probes such as nuclear magnetic resonance (NMR) and muon spin resonance (μSR) on single/polycrystalline samples. These investigations will provide insights into the superconducting pairing mechanism and a better understanding of the possible unconventional nature and anomalous enhancement of the superconducting transition in the $\text{Ta}_x\text{Hf}_{1-x}$ binary alloy.

VI. ACKNOWLEDGMENTS

P. K. Meena acknowledges the funding agency Council of Scientific and Industrial Research (CSIR), Government

of India, for providing the SRF fellowship (Award No: 09/1020(0174)/2019-EMR-I). R. P. S. acknowledges the Science and Engineering Research Board, Government of India, for the Core Research Grant CRG/2019/001028.

-
- [1] J. Bardeen, L. N. Cooper, and J. R. Schrieffer, *Phys. Rev.* 106, 162 (1957).
 - [2] M. Sigrist and K. Ueda, *Rev. Mod. Phys.* 63, 239 (1991).
 - [3] K. Maki, *Phys. Rev.* 148, 362 (1966).
 - [4] G. E. Volovik and L. P. Gorkov, *Sov. Phys. JETP* 61, 843 (1985).
 - [5] P. W. Anderson, *Phys. Rev. B* 30, 4000 (1984).
 - [6] M. Z. Hasan and C. L. Kane, *Rev. Mod. Phys.* 82, 3045 (2010).
 - [7] N. P. Armitage, E. J. Mele, and A. Vishwanath, *Rev. Mod. Phys.* 90, 015001 (2018).
 - [8] X. L. Qi and S. C. Zhang, *Rev. Mod. Phys.* 83, 1057 (2011).
 - [9] M. Sato and Y. Ando, *Rep. Prog. Phys.* 80, 076501 (2017).
 - [10] R. J. Elliott, *Phys. Rev.* 96, 280 (1954).
 - [11] Arushi, K. Motla, P. K. Meena, S. Sharma, D. Singh, P. K. Biswas, A. D. Hillier, and R. P. Singh, *Phys. Rev. B*, 105, 054517 (2022).
 - [12] M. Mandal, C. Patra, A. Kataria, D. Singh, P. K. Biswas, J. S. Lord, A. D. Hillier, and R. P. Singh, *Phys. Rev. B* 104, 054509 (2021).
 - [13] S. Harada, J. J. Zhou, Y. G. Yao, Y. Inada, and G. Q. Zheng, *Phys. Rev. B* 86, 220502(R) (2012).
 - [14] H. Takeya, M. ElMassalami, S. Kasahara, and K. Hirata, *Phys. Rev. B* 76, 104506 (2007).
 - [15] T. Shang, J. Z. Zhao, D. J. Gawryluk, M. Shi, M. Medarde, E. Pomjakushina, and T. Shiroka, *Phys. Rev. B* 101, 214518 (2020).
 - [16] C. Q. Xu, B. Li, J. J. Feng, W. H. Jiao, Y. K. Li, S. W. Liu, Y. X. Zhou, R. Sankar, N. D. Zhigadlo, H. B. Wang, Z. D. Han, B. Qian, W. Ye, W. Zhou, T. Shiroka, P. K. Biswas, X. Xu, and Z. X. Shi, *Phys. Rev. B* 100, 134503 (2019).
 - [17] G. Bian, T. R. Chang, R. Sankar, S. Y. Xu, H. Zheng, T. Neupert, C. K. Chiu, S. M. Huang, G. Chang, I. Belopolski, D. S. Sanchez, M. Neupane, N. Alidoust, C. Liu, B. Wang, C. C. Lee, H. T. Jeng, C. Zhang, Z. Yuan, S. Jia, A. Bansil, F. Chou, H. Lin, and M. Z. Hasan, *Nat. Commun.* 7, 10556 (2016).
 - [18] M. Suenaga and K. M. Ralls, *J. Appl. Phys.* 40, 4457 (1969).
 - [19] R. A. Hein, *Phys. Rev.* 102, 1511 (1956).
 - [20] J. K. Hulm and R. D. Blaugher, *Phys. Rev.* 123, 1569 (1961).
 - [21] A. Birnboim, *Phys. Rev. B* 14(7), 2857 (1976).
 - [22] F. J. Morin and J. P. Maita, *Phys. Rev.* 129, 1115 (1963).
 - [23] S. Sundar, L. S. S. Chandra, M. K. Chattopadhyay, S. K. Pandey, D. Venkateshwarlu, R. Rawat, V. Ganesan, and S. B. Roy, *New. J. Phys.* 17, 053003 (2015).
 - [24] S. Sundar, L. S. Sharath Chandra, M. K. Chattopadhyay, and S. B. Roy, *J. Phys. Condens. Matter* 27, 045701 (2015).
 - [25] J. M. Corsan and A. J. Cook, *Phys. Lett. A* 28 500 (1969).
 - [26] W. Gey and D. Kohnlein, *z. Physik* 255, 308 (1972).

- [27] P. Selvamani, G. Vaitheeswaran, V. Kanchana, M. Rajagopalan, *Physica C* 370, 108 (2002).
- [28] O. De la PenaSeaman, R. de Coss, R. Heid, and K. P. Bohnen, *Phys. Rev. B* 76, 174205 (2007).
- [29] T. G. Berlincourt and R. R. Hake *Phys. Rev.* 131, 140 (1963).
- [30] K. M. Wong, E. J. Cotts, and S. J. Poon, *Phys. Rev. B* 30, 1253 (1984).
- [31] J. RodrÁguez-Carvajal, *Phys. B Cond. Matt.* 192, 55 (1993).
- [32] M. P. Krug, L. L. Oden, and P. A. Romans, *Metall. Trans. A* 6, 997 (1975).
- [33] K. Ma, K. Gornicka, R. LefÁšvre, Y. Yang, H. M. RÁžnow, H. O. Jeschke, T. Klimczuk, and F. O. von Rohr, *ACS Mater. Au* 1, 55 (2021).
- [34] A. A. Castro, O. Olicon, R. Escamilla, and F. Morales, *Solid State Commun.* 255, 11 (2017).
- [35] A. Mani, L. S. Valdhyanathan, Y. Hariharan, M. P. Janawadkar, and T. S. Radhakrishnan, *Cryogenics* 36, 937 (1996).
- [36] M. Matin, L. S. Sharath Chandra, S. K. Pandey, M. K. Chattopadhyay, and S. B. Roy, *Eur. Phys. J. B* 87, 131 (2014).
- [37] S. L. Narasimhan, R. Taggart, and D. H. Polonis, *Journal of Nuclear Materials* 43, 3 (1972).
- [38] H. Yang, H. Luo, Z. Wang, and H. H. Wen, *Appl. Phys. Lett.* 93, 142506 (2008).
- [39] R. Prozorov, N. Ni, M. A. Tanatar, V. G. Kogan, R. T. Gordon, C. Martin, E. C. Blomberg, P. Prommapan, J. Q. Yan, S. L. Budko, and P. C. Canfield, *Phys. Rev. B* 78, 224506 (2008).
- [40] P. K. Biswas, A. Amato, R. Khasanov, H. Luetkens, K. Wang, C. Petrovic, R. M. Cook, M. R. Lees, and E. Morenzoni, *Phys. Rev. B* 90, 144505 (2014).
- [41] D. A. Mayoh, J. A. T. Barker, R. P. Singh, G. Balakrishnan, D. McK. Paul, and M. R. Lees, *Phys. Rev. B* 96, 064521 (2017).
- [42] N. R. Werthamer, E. Helfand, and P. C. Hohenberg, *Phys. Rev.* 147, 295 (1966).
- [43] E. Helfand, and N. R. Werthamer, *Phys. Rev.* 147, 288 (1966).
- [44] B. S. Chandrasekhar, *Appl. Phys. Lett.* 1, 7 (1962).
- [45] A. M. Clogston, *Phys. Rev. Lett.* 9, 266 (1962).
- [46] A. Kataria, T. Agarwal, S. Sharma, A. Ali, R. S. Singh, and R. P. Singh, *Supercond. Sci. Technol.* 35, 115008 (2022).
- [47] M. Mandal, K. P. Sajilesh, R. R. Chowdhury, D. Singh, P. K. Biswas, A. D. Hillier, and R. P. Singh, *Phys. Rev. B* 103, 054501 (2021).
- [48] D. Singh, P. K. Biswas, A. D. Hillier, and R. P. Singh, *Phys. Rev. B* 101, 144508 (2020).
- [49] H. Su, T. Shang, F. Du, C. F. Chen, H. Q. Ye, X. Lu, C. Cao, M. Smidman, and H. Q. Yuan, *Phys. Rev. Materials* 5, 114802 (2021).
- [50] K. P. Sajilesh, K. Motla, P. K. Meena, A. Kataria, C. Patra, K. Somesh, A. D. Hillier, and R. P. Singh, *Phys. Rev. B* 105, 094523 (2022).
- [51] M. Tinkham, *Introduction to Superconductivity*, 2nd ed. (McGraw - Hill, New York, 1996).
- [52] M. Mandal, S. Marik, K. P. Sajilesh, Arushi, D. Singh, J. Chakraborty, N. Ganguli, and R. P. Singh, *Phys. Rev. Materials* 2, 094201 (2018).
- [53] S. Chakraborty, R. Kumar, and N. Mohapatra, *Phys. Rev. B* 107, 024503 (2023).
- [54] I. K. Dimitrov, N. D. Daniilidis, C. Elbaum, J. W. Lynn, and X. S. Ling, *Phys. Rev. Lett.* 99, 047001 (2007).
- [55] C. Kittel, *Introduction to Solid State Physics*, 8th ed. (John Wiley & Sons, Hoboken, NJ, 2005).
- [56] W. L. McMillan, *Phys. Rev.* 167, 331 (1968).
- [57] T. Shang, D. J. Gawryluk, J. A. T. Verezhak, E. Pomjakushina, M. Shi, M. Medarde, J. Mesot, and T. Shiroka, *Phys. Rev. Materials* 3, 024801 (2019).
- [58] R. W. Rollins and Lavern C. Clune, *Phys. Rev. B* 6, 2609 (1972).
- [59] H. Padamsee, J. E. Neighbor, C. A. Shiffman, J. Low. Temp. Phys. 12 (3), 387 (1973).
- [60] D. A. Mayoh, J. A. T. Barker, R. P. Singh, G. Balakrishnan, D. McK. Paul, and M. R. Lees, *Phys. Rev. B* 96, 064521 (2017).
- [61] A. D. Hillier, and R. Cywinski, *Appl. Magn. Reson.* 13, 95 (1997).
- [62] Y. J. Uemura, G. M. Luke, B. J. Sternlieb, J. H. Brewer, J. F. Carolan, W. N. Hardy, R. Kadono, J. R. Kempton, R. F. Kiefl, S. R. Kreitzman, P. Mulhern, T. M. Riseman, D. L. Williams, B. X. Yang, S. Uchida, H. Takagi, J. Gopalakrishnan, A. W. Sleight, M. A. Subramanian, C. L. Chien, M. Z. Cieplak, G. Xiao, V. Y. Lee, B. W. Statt, C. E. Stronach, W. J. Kossler, and X. H. Yu, *Phys. Rev. Lett.* 62, 2317 (1989).
- [63] T. Mamiya, K. Nomura, and Y. Masuda, *J. Phys. Soc. Jpn.* 28, 380 (1970).
- [64] J. J. Hopfield, *Phys. Rev.* 186, 443 (1969).
- [65] C. K. Jones, J. K. Hulm, and B. S. Chandrasekhar, *Rev. Mod. Phys.* 36, 74 (1964).